Mon. Not. R. Astron. Soc. **000**, 000–000 (0000) Printed 16 November 1999 (MN plain TEX macros v1.6)

The ROSAT International X-ray Optical Survey (RIXOS): source catalogue

K. O. Mason,[1] F. J. Carrera,[1,2] G. Hasinger,[3] H. Andernach,[4]
A. Aragon-Salamanca,[5] X. Barcons,[2] R. Bower,[6] W. N. Brandt,[7]
G. Branduardi-Raymont,[1] J. Burgos-Martín,[8] F. Cabrera-Guerra,[8]
R. Carballo,[2,9] F. Castander,[5] R. S. Ellis,[5] J. I. González-Serrano,[2]
E. Martínez-González,[2] J. M. Martín-Mirones,[9] R. G. McMahon,[5]
J. P. D. Mittaz,[1] K. L. Nicholson,[1] M. J. Page,[1] I. Pérez-Fournon,[8]
E. M. Puchnarewicz,[1] E. Romero-Colmenero,[1] A. D. Schwope,[3] B. Vila,[8]
M. G. Watson,[10] D. Wonnacott[1]

[1] *Mullard Space Science Laboratory, University College London, Holmbury St. Mary, Dorking, Surrey RH5 6NT, UK.*
[2] *Instituto de Física de Cantabria, Consejo Superior de Investigaciones Científicas-Universidad de Cantabria, Santander, Spain.*
[3] *Astrophysikalisches Institut Potsdam, An der Sternwarte 16, 14482 Potsdam, Germany.*
[4] *Depto. de Astronomia, IFUG, Guanajuato, Mexico.*
[5] *Institute of Astronomy, Madingley Road, Cambridge, UK.*
[6] *Physics Dept., University of Durham, Durham DH1 3LE, UK.*
[7] *Astronomy Dept., Pennsylvania State University, 525 Davey Lab, University Park, PA 16802, USA.*
[8] *Instituto de Astrofísica de Canarias, La Laguna, Tenerife, Spain.*
[9] *Dpto. de Fisica Moderna, Universidad de Cantabria, Santander, Spain*
[10] *Dept. of Physics and Astronomy, University of Leicester, Leicester, LE1 7RH, UK*

ABSTRACT

We describe the ROSAT International X-ray/Optical Survey (RIXOS), a medium sensitivity survey and optical identification of X-ray sources discovered in ROSAT high Galactic latitude fields ($|\ b\ |>28°$) and observed with the Position Sensitive Proportional Counter (PSPC) detector. The survey made use of the central 17 arc minutes of each ROSAT field. A flux limit of 3×10^{-14} erg cm^{-2} s^{-1} (0.5-2 keV) was adopted for the survey and a minimum exposure time of 8000 seconds was required for qualifying ROSAT observations. X-ray sources in the survey are therefore substantially above the detection threshold of each field used, and many contain enough counts to allow the X-ray spectral slope to be estimated.

Spectroscopic observations of potential counterparts were obtained of all sources down to the survey limit in 64 fields, totalling a sky area of 15.77 deg^2. Positive optical identifications were made for 94% of the 296 source thus examined. A further 18 fields (4.44 deg^2), containing 105 sources above the 3×10^{-14} erg cm^{-2} s^{-1} survey limit, are completely optically identified to a higher flux of 8×10^{-14} erg cm^{-2} s^{-1} (0.5-2 keV). Optical spectroscopic data is supplemented by deep CCD imaging of many sources to reveal the morphology of the optical counterparts, and objects too faint to register on Sky Survey plates. The faintest optical counterparts have R$\sim$22.

This paper describes the survey method and presents a catalogue of the RIXOS sources and their optical indentifications. Finding charts based on sky survey data are given for each source, supplemented by CCD imaging where necessary.

Key words: Surveys - X-rays: general - Galaxies: active - Galaxies: clustering - quasars: general - Stars: late-type

1 INTRODUCTION

Since its launch in 1990, the *ROSAT* satellite (Trümper 1983) has proved to be of major value in studying faint X-ray source populations. With its good imaging quality and low instrumental background the X-ray telescope on *ROSAT* has amply fulfilled its promise as a survey instrument, delivering images of the X-ray sky which have unprecedented sensitivity. *ROSAT* conducted a scanning survey of the entire sky, mostly during the first six months of its operation, and has completed many thousand pointed observations since. The all-sky survey reached a depth of better than about 5×10^{-13} erg cm^{-2} s^{-1} in the 0.5-2.0 keV band (Voges et al. 1998), while the deepest pointed observations detect sources down to $\sim 2 \times 10^{-15}$ erg cm^{-2} s^{-1} (McHardy et al. 1998; Hasinger et al. 1998). Such observations provide a census of X-ray sources and population types. Among other things, they can be used to investigate the evolution of extragalactic sources, and to form statistical samples of objects for studying the physics of their emission processes.

At the deepest flux levels that *ROSAT* can reach, source densities on the high Galactic latitude sky are about 500 per square degree, but this drops to only 0.5 per square degree at a flux of 5×10^{-13} erg cm^{-2} s^{-1} (0.5-2 keV). Thus in order to register significant numbers of sources with intermediate fluxes, data from several ROSAT fields are required. The RIXOS survey, described in this paper, addresses this intermediate flux regime by assembling a sample of almost 300 sources brighter than 3×10^{-14} erg cm^{-2} s^{-1} (0.5-2 keV) taken from 64 *ROSAT* pointed observations. Optical identifications for this sample, which is refered to as RIXOS3 and covers in total 15.77 square degrees of sky, are 94% complete. We also include data on a further 4.44 square degrees of sky which is completely optically identified to a flux level of 8×10^{-14} erg cm^{-2} s^{-1} and refered to as RIXOS8.

In addition to the deep surveys noted above, other surveys of ROSAT sources in the literature include the QSF survey (Shanks et al. 1991), the Cambridge-Cambridge ROSAT Serendipitous Survey (Boyle et al. 1995) and the UK Medium Survey (Carballo et al. 1995). These extend to fainter flux limits than RIXOS, at various levels of completeness, but cover a smaller sky area.

The nearest precedent to RIXOS is the Einstein Extended Medium Sensitivity Survey (Stocke et al. 1991) that included ~800 sources over ~800 deg^2, with very different flux limits, ranging from 3×10^{-12} to 5×10^{-14} erg cm^{-2} s^{-1} in the 0.3-3.5 keV band.

2 SURVEY METHOD

To assemble the sample of X-ray sources used in RIXOS we chose ROSAT PSPC fields which had exposure times of at least 8000s. This ensures that sources at our intended survey flux limit of 3×10^{-14} erg cm^{-2} s^{-1} (0.5–2.0 keV) lie significantly above the sensitivity threshold of every field. We also limit the choice of fields to those which have Galactic latitude greater than 28° in either hemisphere since RIXOS is primarily intended for extragalactic source studies. Though not a formal selection criterion, the Galactic absorbing column density in RIXOS fields (see Table 1) is generally no more than a few times 10^{20} H atoms cm^{-2} based on the data of Stark et al. (1992), so attenuation of the source signal above 0.5 kev is never severe.

We eliminate from consideration fields which have bright and/or extended targets which might increase the overall background level against which to search for field sources. Only data within 17 arc minutes of the field centre are used to ensure the best X-ray image quality and the most accurate source positions. The target of the observation (where there was one) was excluded from the survey together with any area around it that was contaminated by its point spread function (typically 2-3 arc minutes radius, see Table 1). In a number of fields either there was no target, the target was further than 20 arcmin offaxis, or the target was not detected. In these cases we did not exclude any part of the central area from our analysis.

A total of 94 ROSAT fields (a mixture of Rev. 0 and Rev. 1 data) were selected as being suiTable for RIXOS. When more than one ROSAT observations were available for a given field, the corresponding images were coadded prior to the source search to maximize the sensitivity of the survey. Significant optical identification work was subsequently carried out in 82 fields (including three fields that had no sources down to our X-ray flux limit). The fields used are listed in Table 1 along with relevant ancillary information.

In applying the survey flux cutoff of 3×10^{-14} erg cm^{-2} s^{-1} (0.5–2.0 keV) we assumed a conversion from source counts to flux which was appropriate for a power law source spectrum with an energy index, α, of –1 (defined here and throughout such that $F_\nu \propto \nu^\alpha$), and corrected for the (usually small) effects of Galactic absorption. Such a conversion factor is appropriate for quasars (Mittaz et al. 1999) but may systematically under- or over-estimate the flux of other source classes.

Because the flux threshold for RIXOS was set at a value significantly above the sensitivity threshold of the individual fields used, many RIXOS sources have sufficient counts to allow us to measure their X-ray spectral slope individually. This work was done subsequent to the definition of the catalogue and is described by Mittaz et al. (1999). This allowed us to get an (in principle) improved estimate of the source flux based on a power-law spectral fit to the *ROSAT* PSPC data collected in three broad energy channels (the Galactic neutral hydrogen absorption has been taken into account for the fits to the extragalactic sources, but the fluxes given are what they would be before absorption by the Galaxy). In the cases in which more than one observations were used to create the image to be source searched, the longest single exposure time observation was chosen for the spectral analysis.

2.1 X-ray source detection

The RIXOS X-ray images (in PHA channels 52-201) have been analysed using an improved version of the interactive analysis system EXSAS (Zimmermann et al. 1994). The first steps of the detection procedure, i.e. the local detect algorithm LDETECT, the bicubic spline fit to the background map and the map detection algorithm MDETECT have been described in Hasinger et al. (1993). The detection threshold of these algorithms has been set at a very low likelihood value so that the resulting list of possible source positions contains several hundred spurious detections. This position list has then been fed into the "multi–ML" crowded field detection and parameter estimation algorithm first described by Hasinger et al. (1994a). This method, which has been implemented in EXSAS, works on binned image data and fits superpositions of several PSF profiles on top of an external background to sections of the data (typically sub–images of arcmin size). Best–fit positions and normalizations are obtained by maximizing the likelihood statistic $\mathcal{L}$ (Cash 1979) or, correspondingly, by minimizing the quantity

$$\mathcal{S} = -2ln\mathcal{L} = -2\sum_{i,j}(Y_{mod}(i,j) - N(i,j)lnY_{mod}(i,j)$$

$Y_{mod}(i,j)$ is the sum of all model point source contributions plus the background value in the image pixel [i,j] and N is the measured number of photons in pixel [i,j]. For ROSAT PSPC data the multi–component PSF (Hasinger et al., 1994b; David et al., 1996) is approximated by a single

Table 1. ROSAT fields used in the RIXOS survey

Fid	ROR	$N_{\rm H}$ 10^{20} H atoms cm^{-2}	Exp Time (s)	Spec Time (s)	RA (2000)	Dec (2000)	Radius (')	Total	ID	P	Target
(1)	(2)	(3)	(4)	(5)	(6)	(7)	(8)	(9)	(10)	(11)	(12)
*281	P701092	5.76	9117	8442	00 10 29	10 58 12	2.67	3	3	0	[HB89] 0007+106
*262	P701048	3.37	13894	12819	01 24 34	03 47 60	2.67	5	5	0	NGC 520
292	P200468	3.48	8663	7095	01 43 22	04 19 48	2.67	5	3	1	GJ 70
246	P300003	6.19	25174	22472	02 06 53	15 18 00	4.00	8	2	3	TT Ari
*245	P700099	8.81	25727	23607	03 28 27	02 48 00	0.00	3	2	1	[HB89] 0323+022
279	P700531	4.28	9547	7636	03 53 48	-10 25 12	0.00	7	3	1	BR 0351-1034
270	P700271	3.57	10879	8081	04 05 34	-13 08 24	2.67	6	3	2	[HB89] 0403-132
*283	P701055	10.46	9043	6147	04 16 53	01 05 24	4.00	8	4	3	[HB89] 0414+009
*211	P700210	3.95	21043	14298	07 21 53	71 20 24	2.67	7	6	1	[HB89] 0716+714
*234	P700112	4.05	19844	15658	07 42 41	65 10 48	1.33	3	3	0	Mkn 78
*255	P700315	5.07	15992	7361	07 58 29	37 47 24	4.00	7	4	3	NGC 2484
*213	P700258	4.35	8354	6269	08 04 31	65 00 00	0.00	7	6	1	[HB89] 0759+651
*293	P200473	4.59	8954	7098	08 19 48	37 31 12	0.00	7	6	1	GD 90
*206	P200453	3.65	15927	13559	08 26 53	26 37 48	4.00	5	5	0	DX Cnc
*228	P400020	3.66	10978	9297	08 38 48	36 31 12	2.67	5	3	2	GBS0839+37
*221	P700546	2.90	12391	9932	08 48 19	37 40 12	2.67	6	5	1	[HB89] 0845+378
304	P700887	3.56	18552	17732	08 53 10	13 52 48	2.67	9	4	3	[HB89] 0850+140
250	P700436	3.52	21565	19372	08 58 41	14 08 60	2.67	7	1	2	[HB89] 0855+143
*257	P700326	2.18	14511	11469	09 05 31	34 07 48	0.00	6	5	0	B2 0902+343
*248	P700329	1.50	23561	19550	09 09 34	42 54 00	2.67	4	2	0	[HB89] 0906+430
*216	P700211	3.54	19495	14701	09 21 36	62 15 36	2.67	5	4	1	87GB 091738.6+622823
299	P700262	1.56	10298	8011	09 25 12	52 17 24	2.67	2	1	0	Mkn 110
*290	P700389	1.46	8158	6669	09 39 53	35 54 00	2.67	2	2	0	3C 223.0
*253	P700387	1.59	17193	14814	09 41 05	38 54 00	2.67	2	2	0	[HB89] 0937+391
*285	P400141	3.43	8957	8190	09 43 43	16 31 12	0.00	4	2	1	PSR 0940+16
*305	P701214	2.25	12532	8353	09 49 46	73 14 24	2.67	6	3	2	87GB 094429.5+732721
*218	P400059	3.01	9038	5371	09 53 10	07 55 48	2.67	6	6	0	PSR 0950+08
*252	P700319	0.78	19006	11893	10 01 58	55 40 48	5.33	7	7	0	NGC 3079
*286	P700774	2.33	8868	7406	10 04 19	05 13 12	0.00	3	2	1	[HB89] 1001+054
*232	P900214	0.84	15911	11651	10 10 12	50 45 00	0.00	3	2	1	UKMS Field, no target
230	P700265	0.79	23995	18778	10 10 14	51 45 00	0.00	3	0	0	UKMS Field, no target
229	P700263	0.79	14616	12287	10 10 14	52 45 00	0.00	5	4	0	UKMS Field, no target
*208	P700264	0.73	17331	15224	10 10 17	53 45 00	0.00	5	3	1	UKMS Field, no target
231	P900213	0.73	16813	10890	10 10 17	54 45 00	0.00	7	4	2	UKMS Field, no target
*115	P000049	2.50	38910	-[a]	10 11 00	28 15 00	0.00	2	1	0	Nowhere, no target
*225	P200076	2.19	26522	18123	10 19 38	19 52 12	2.67	1	1	0	AD Leo
*302	P700540	1.23	19359	10041	10 24 34	47 09 00	0.00	3	2	1	IRAS 10214+4724
*273	P700384	2.81	10209	5172	10 42 46	12 03 36	2.67	7	6	0	[HB89] 1040+123
*260	P300158	0.93	14008	9962	10 47 14	54 18 36	0.00	4	4	0	EK UMa
*133	P300137	1.19	9400	6167	10 56 55	49 42 00	2.67	4	4	0	CY UMa
*291	P200127	2.02	16670	-[c]	11 03 24	36 02 24	2.67	0	0	0	HD 95735
303	P700872	3.55	13081	9962	11 06 47	72 34 12	2.67	6	4	0	NGC 3516
*258	P700358	3.36	14425	13035	11 18 17	07 46 12	1.47	6	6	0	[HB89] 1115+080
*123	P700228	1.22	24950	19887	11 19 05	21 18 36	4.00	11	10	0	PG 1116+215
*259	P700010	1.96	14061	10545	11 20 17	13 35 24	4.00	5	4	1	NGC 3628
*271	P700510	2.07	10676	5785	11 24 43	38 45 36	2.67	3	2	1	NGC 3665
*287	P700499	1.06	8827	8827	11 25 36	54 22 48	1.47	1	1	0	Mkn 40
*251	P700372	4.44	21284	-[c]	11 29 17	-04 24 00	2.67	0	0	0	Mkn 1298

Gaussian function with a width increasing with off–axis angle. The significance $\Delta\mathcal{S}$ of any of the individual point source contributions is then estimated by a likelihood ratio test between the best fit with and without the corresponding component. If $\Delta\mathcal{S}$ falls below a threshold value, the corresponding component is omitted from the next iteration and only significant components are maintained. Since $\Delta\mathcal{S}$ follows a χ^2 distribution, the errors of the best–fit parameters (68% confidence single parameter of interest) are determined by searching the parameter space for which $\Delta\mathcal{S} = \mathcal{S} - \mathcal{S}_{min} = 1$. Before the next region of interest is fit, the current PSF contributions are added to the background model.

The complete source detection and parameter estimation procedure is too complicated to validate its results and e.g. quantify its detection efficiency analytically. We therefore performed extensive simulations of artificial ROSAT fields run through the same set of algorithms to study their properties. Based on these simulations we have chosen a likelihood detection threshold of $\Delta\mathcal{S} = 10$, corresponding to a 4σ detection. We emphasise however that our survey sensitivity limit of 3×10^{-14} erg cm^{-2} s^{-1} is substantially above the detection threshold in all fields. Observed fluxes

Table 1 *(cont.)* ROSAT fields used in the RIXOS survey

Fid (1)	ROR (2)	N_H 10^{20} H atoms cm^{-2} (3)	Exp Time (s) (4)	Spec Time (s) (5)	RA (2000) (6)	Dec (2000) (7)	Radius (') (8)	Total (9)	ID (10)	P (11)	Target (12)
*227	P200091	1.77	33886	25321	11 36 34	29 47 60	0.00	4	3	1	GD 140
*240	P700055	1.22	58534	50084	11 57 56	55 27 14	5.33	4	4	0	NGC 3998
222	P701202	2.43	13563	12885	12 01 14	-03 40 48	2.67	5	2	1	Mkn 1310
*116	P000054	1.22	30590	-[a]	12 03 60	56 10 12	0.00	3	3	0	Nowhere, no target
124	P700232	1.64	17400	13651	12 04 41	27 53 60	2.67	5	2	0	[HB89] 1202+281
127	P700221	1.71	22400	20207	12 17 55	30 06 36	2.67	11	4	2	[HB89] 1215+303
*126	P700223	1.95	10400	10795	12 21 34	28 13 48	2.67	3	2	1	ON 231
288	P700506	1.43	8820	6773	12 28 24	31 28 48	2.67	5	1	0	[HB89] 1225+317
266	P700435	2.05	12299	8351	12 32 02	20 09 36	2.67	6	4	1	Mkn 771
*219	P700208	1.29	24340	20172	12 56 14	56 52 12	2.67	6	4	2	UGC 8058,Mkn 231
*226	P700073	1.19	48051	38128	12 56 58	47 20 24	1.07	6	4	2	3C 280
*265	P700216	1.10	13034	12024	13 10 29	32 20 60	2.67	6	5	0	[HB89] 1308+326
*224	P100308	1.01	34943	19366[b]	13 16 24	29 06 00	2.67	3	2	1	HZ43
*278	P701034	1.94	9611	9023	13 32 24	11 06 36	2.67	4	3	1	Mkn 789
277	P700473	1.74	9918	8995	13 38 17	48 16 48	2.67	9	5	1	NGC 5256
*254	P700391	1.05	17116	9076	13 44 43	55 53 24	1.07	5	5	0	Mkn 273
*268	P700392	2.08	11553	10090	13 56 02	18 22 12	2.67	4	2	2	Mkn 463
*274	P700227	2.16	10141	4581	14 06 22	22 23 60	2.67	1	1	0	PG 1404+226
*249	P700117	1.20	22692	-[c]	14 06 43	34 11 23	2.67	0	0	0	C 294
*217	P700248	1.13	25319	21739	14 13 48	44 00 00	2.67	7	7	0	PG 1411+442
*215	P150046	1.18	11516	8434	14 19 46	54 23 24	2.67	4	3	1	[HB89] 1418+546
*110	P200329	1.07	18250	23688	14 28 43	33 10 45	0.00	5	5	0	LHS2924
*261	P201103	3.31	13937	12855	15 34 41	26 43 12	2.67	2	0	2	HR 5793
237	P700230	2.95	8442	6370	16 13 58	65 43 12	2.67	2	1	0	[HB89] 1613+658
*122	P170174	4.12	38450	30325[b]	16 29 24	78 04 48	4.00	8	7	1	2RE J162911.2+780443
*212	P700255	1.19	8933	6878	16 30 19	37 19 12	0.00	5	5	0	[HB89] 1628+374
*223	P200721	1.84	47467	37173	16 34 24	57 09 00	2.67	5	3	1	CM Dra
*238	P700246	4.08	9357	7654	16 34 29	70 31 48	2.67	6	2	1	[HB89] 1634+706
*236	P700123	2.55	8196	4946	17 01 24	51 49 12	0.00	4	3	0	[HB89] 1700+518
*220	P701200	3.94	10578	6364	17 26 12	74 31 12	2.67	8	8	0	RX J1726.2+7431
*272	P700489	4.67	10461	7378	18 06 50	69 49 12	2.67	9	7	2	[HB89] 1807+698
*205	P100578	4.31	10313	9624	23 12 22	10 46 48	4.00	6	5	0	BPM 97859
*294	P200474	4.25	9488	9227	23 18 46	12 36 00	0.00	3	3	0	KUV 23162+1220
*125	P200322	5.04	26300	22513	23 25 19	23 24 36	4.00	3	2	1	HR 8905

Column 1: RIXOS field ID (Fid). Fields marked with a '*' constitute the RIXOS3 sample (see section 4). **Column 2:** ROSAT observation request number. **Column 3:** Galactic absorbing column in the direction of the field centre derived from Stark et al. (1992). **Column 4:** Total ROSAT exposure time used for the detection. **Column 5:** ROSAT exposure time used for the spectral analysis. **Column 6 & 7:** J2000 coordinates of field centre. **Column 8:** Excluded radius around the target. **Columns 9-11:** Respectively, the total number of RIXOS sources in the field, the number of secure identifications, and the number of probable identifications. **Column 12:** Name of the ROSAT target.

[a]: No ROSAT public data available at the time of the spectral analysis.

[b]: Detection image coadded from several individual images. The ROR number given correspond to the single longest exposure, that was also used for the spectral analysis.

[c]: No spectral analysis performed because no sources were detected in this field above the survey flux limit.

in the 0.5–2 keV band are calculated for each source using the detected counts, the corresponding exposure time and vignetting correction, an energy–to–flux conversion factor (ECF) and a PSF–loss correction factor (PCF) determined from simulations. In order to derive the ECF we assumed a power law spectrum with energy index -1 and galactic absorption, folded through the instrument response.

The source detection algorithm is optimised for point sources. Subsequent to running the automatic detection algorithm, all fields were visually inspected for clusters of point sources which could indicate that there is actually an underlying extended source present. In such cases the source flux was aggregated into a single source whose position was taken to be the centroid of the counts. The corresponding uncertainty in the position was taken to be the radius that would include most of the counts of the merged source.

After the first pass through the detection algorithm each source was assigned a number which was preserved through the whole of the remaining process even though many of these sources were dropped in subsequent steps of the procedure. Internally within the RIXOS programme sources were referred to by this number (Sid) qualified by the field number listed in Table 1 (Fid). Sources believed to be extended as described in the previous paragraph were assigned Sid numbers by adding 500 to the Sid number of the brightest component point source. All sources with Sid>500 are in this category.

Table 3. Catalogue identifications of RIXOS Sources

RIXOS Source	Catalogue identification
RX J001002.5+110837	BD+10 8B, HD560B, MS0007.4+1051
RX J012433.2+034334	[HB89] 0121+034
RX J012457.3+035347	[HB89] 0122+035
RX J020608.5+151235	IC 1777
RX J020619.1+150341	AG+14 185
RX J032754.0+023344	UGC 02748
RX J040523.4-125936	HD 25853
RX J040534.9-125842	SHK 278:[dM91] 04
RX J041612.1+011432	HD 27007
RX J071858.8+712432	87GB 071317.6+712947 (radio source)
RX J072001.6+711524	AG+71 238
RX J072014.5+713228	Zw0714.8+7140
RX J080309.3+650808	HD 65497
RX J082007.6+372840	IRAS F08168+3738
RX J082733.7+263716	87GB 082432.4+264636 (radio source)
RX J084715.7+373214	[HB89] 0844+377
RX J084907.0+373158	A708
RX J085340.3+134927	MS0850.8+1401
RX J085345.5+134948	HD 75976
RX J090926.5+424228	[HB89] 0906+429
RX J091049.4+430407	B3 0907+432 (radio source)
RX J094614.5+732034	AG+73 264
RX J095253.8+075042	[HB89] 0950+080, MS 0950.2+0804
RX J100110.2+552835	[HB89] 0957+557
RX J100120.3+555349	[HB89] 0957+561A,B
RX J100447.7+050016	HD 87392
RX J100454.8+050418	UGC 05432
RX J100953.8+510049	HD 233710
RX J105813.1+493927	[HB89] 1055+499
RX J110741.4+723235	[HB89] 1104+728
RX J112106.0+133825	[HB89] 1118+139
RX J112337.1+384140	HD 98969
RX J113655.3+295131	[HB89] 1134+301
RX J115951.8+553231	MS 1157.3+5548
RX J120108.9-033423	HD104368
RX J120403.2+280715	MS 1201.5+2824
RX J121832.6+301443	HD107054
RX J122907.4+312329	HD108693
RX J123118.4+201308	HD108984
RX J123154.9+195309	4C +20.30? (see sect. 3.2)
RX J123225.3+202316	1E 1229.9+2039, EXO122956+2039.8
RX J125612.1+472113	AG+47 995
RX J125639.4+471519	B3 1254+475 (radio source)
RX J125645.9+570726	HD238172
RX J125738.4+472759	BD+48 2069A,B
RX J131058.8+323335	87GB 130837.7+324939 (radio source)
RX J131112.2+322907	MS 1308.8+3244
RX J133740.5+480758	GJ520B
RX J133751.1+480815	GJ520A
RX J134334.1+553644	A1783
RX J141231.5+435539	IRAS14105+4409
RX J153350.9+264229	AG+26 1493, AG+26 1494
RX J153441.0+265443	AG+27 1450
RX J163239.0+781152	NGC 6217
RX J180434.6+693742	IPC180506+6937
RX J180530.7+694516	EF Dra, 1E 1806.0+6944
RX J180603.7+694024	MS 1806.5+6939
RX J232509.8+233017	HD220626

2.2 Previously catalogued sources

The NED and SIMBAD databases were searched for known objects within 5 arc minutes of the position of each RIXOS X-ray source. All the correlations were then checked manually taking into account the RIXOS and catalogued positional errors, and consulting the relevant references in NED and SIMBAD.

When the identification was uncertain (or irrelevant for our identification programme, eg. a radio source of unknown ID with no redshift), the RIXOS X-ray source was selected for optical spectroscopy and treated like any other source in the sample.

The X-ray sources in RIXOS with likely catalogued counterparts are flagged in the main RIXOS catalogue, Table 2, and the counterparts are listed in Table 3.

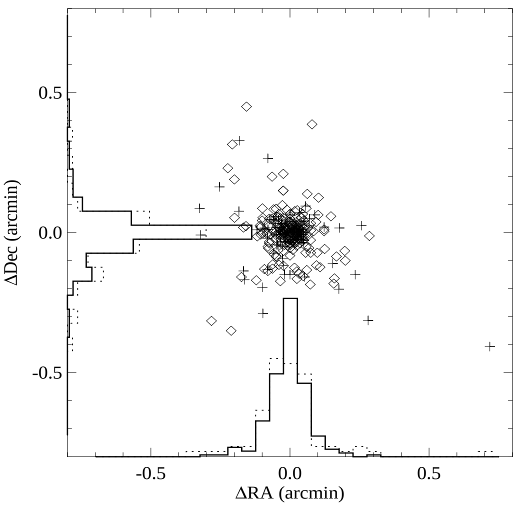

Figure 1. Positional offsets of secure point-like optical counterparts with respect to the X-ray source centroid. Diamonds are AGN, crosses are stars. The distribution of positional offsets projected onto each of the Right Ascension and Declination axes are plotted as histograms, the solid line being AGN and the broken line stars.

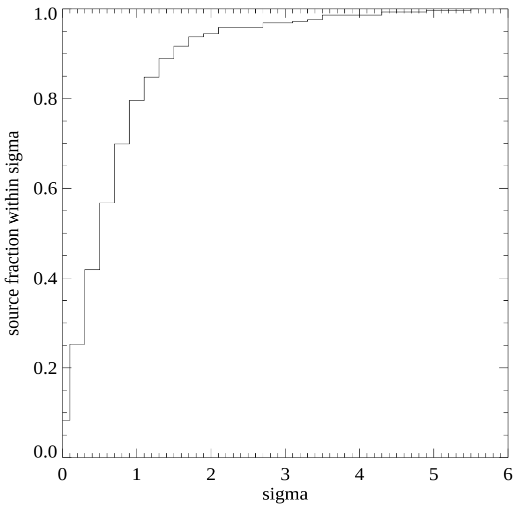

Figure 2. Cumulative distribution of positional offsets for secure point-like RIXOS sources (AGN+stars). The fraction of sources whose separation from the X-ray centroid is less than a given value is plotted against the separation, expressed in units of the 1-sigma error radius.

2.3 Optical identification

As a first stage in the optical identification process, the X-ray source positions were superimposed on Palomar Observatory Sky Survey (POSS) images using parameterised data derived from measurements made with the Automated Plate Measuring (APM) machine at Cambridge (Lewis & Irwin 1996).

The primary means of determining the nature of each X-ray source was through optical spectroscopy. Low resolution spectra were taken of optical targets close to the X-ray position to search for known classes of X-ray emitter. The search radius was extended until such an optical counterpart was found, or until the separation of the X-ray and optical positions became such that association was unlikely.

For well defined point-like X-ray sources the limiting separation was generally taken to be about 30-40 arcsec for extragalactic counterparts, a number that was established at the beginning of the programme based on experience with the first identifications. For stars we allowed some extra distance to account for the possibility of proper motion, unless we had a recent image of the field.

We can verify our assumptions *post facto* by examining the distribution of optical counterpart positions from the full catalogue with respect to each X-ray centroid. Fig. 1 shows the two-dimensional distribution of offsets for AGN and stellar counterparts, classes of sources that are expected to be point-like. This diagram illustrates that the large majority of such sources are found within about 6 arcsec of the X-ray position. Fig. 2 shows similar information, but as a cumulative distribution of offsets expressed in units of the 1 sigma error radius of each source, derived from the X-ray source fitting algorithm.

Account was also taken of the morphology of the X-ray source in setting the radius within which optical counterparts were sought, specifically whether the X-ray source was extended and whether it may be affected by source confusion. For instance, in some cases sources which are formally classified by the X-ray detection algorithm as single objects are clearly elongated in shape. This suggests that they may in fact be two sources closely separated on the sky. In these cases the area searched for optical counterparts was modified to allow for this possibility. This is important in reducing the number of potentially spurious 'blank fields' which could otherwise occur if the counterpart search was confined to the X-ray centroid of closely coincident sources.

In cases where there is more than one potential counterpart within the X-ray search radius, we endeavoured to take optical spectra of them all irrespective of whether a plausible counterpart had already been found. In this way we were sensitive to possible multiple counterparts such as dMe star pairs, gravitationally lensed quasars and galaxy clusters.

The low-resolution spectroscopy was supplemented by higher resolution work aimed at confirming chromospheric activity in bright stellar counterparts.

A parallel programme of optical CCD imaging was undertaken to complement the optical spectroscopy. The primary goal of this programme was to reveal optical counterparts that were below the sky survey plate limit. X-ray sources were scheduled for imaging studies such that those without obvious optical counterparts on the sky survey were given highest priority. The optical imaging programme also proved valuable in identifying or confirming the presence of faint galaxy clusters. The overall RIXOS identification work evolved responsively, such that information from the imaging programme was fed back rapidly to the spectroscopy programme and *vice versa*. This was facilitated by a near real-time first-cut reduction of the data, the products of which were held in a database that was available to each observer at the telescope and to personnel at their home institute who planned each observing run.

The default passband for the RIXOS imaging was the Johnson R filter. Additional passbands (U, B, V & I) were also used as necessary.

2.4 Instrumentation

The RIXOS optical identification work was facilitated by an award of "International Time" on the La Palma telescopes by the Comite Científico International, the body that oversees use of Canarian astronomical telescopes. In this scheme up to 5% of the total schedulable observing time is given over annually to a programme that involves collaboration between countries with interests in the Canarian observatories. The telescopes used for RIXOS were the three that comprise the Isaac Newton Group, namely the 4.2m William Herschel Telescope (WHT), the 2.5m Isaac Newton Telescope (INT) and the 1.0m Jacobus Kapteyn Telescope (JKT), and the 2.5m Nordic Optical Telescope (NOT). The observational programme was carried out in several observing runs in three observing semesters in the interval February 1993 to March 1995.

All the spectroscopy was done on either the WHT or INT, while the primary telescopes used for the imaging programme were the NOT, INT and JKT, with limited deep imaging also being conducted on the WHT.

2.4.1 Spectroscopy

The WHT spectroscopy utilised the twin-armed ISIS spectrograph. The input starlight is separated into blue and red beams by a dichroic filter which, for the RIXOS programme had a crossover wavelength of 5400Å. Each of the two spectrograph arms was equipped with a TEK 1124×1124 CCD chip. In the standard configuration used in the low-resolution RIXOS work, the blue spectrograph arm was equipped with the R300B grating, which yielded spectra with a dispersion of approximately 1.5Å/pixel. The R158R grating was used in the red arm yielding approximately 2.5Å/pixel. The lower threshold of the blue grating was set at 3700Å while the upper threshold of the red grating was set at 8400Å. This configuration provided some overlap to aid cross-calibration of the two arms.

Much of the INT spectroscopy utilised the Faint Object Spectrograph (FOS), a crossed dispersed fixed format spectrograph that yields spectral coverage between the atmospheric cut-off and $\sim 1\mu$m in two orders. Spectral resolution is 16Å in the red (first order), and 8Å in the blue. FOS was unavailable for the final RIXOS runs. Instead we used the Intermediate Dispersion Spectrograph (IDS) with the R150V grating and a TEK 1124×1124 CCD chip. This gave coverage between 3600Å and $\sim 1\mu$m, but with some contamination longward of 8000Å due to second order light.

Some RIXOS sources have bright stars in or near their X-ray error circles, many of which have not previously been recorded as 'active'. In order to search for line emission indicative of chromospheric activity, and confirm that the star was the source of the X-ray emission, we recorded some higher resolution spectra of such stars using the IDS. These covered the CaII H&K lines (3934Å, 3963Å) and the Hα line in separate exposures.

All spectroscopy of single objects was done where possible with the slit at or close to the parallactic angle to avoid colour-dependent light loss. Occasionally, to maximise observing efficiency, the spectrograph slit was orientated to as to place two (or more) nearby objects on the slit together. In such cases, however, we tried to ensure that the observations were made at low zenith distance, to minimise differential refraction effects.

2.4.2 Imaging

Several RIXOS fields were imaged in the R band at the beginning of the programme with the FORD CCD camera on the INT. This 2048×2048 device covers a large field of view (11 arc minutes) so that the whole of the central region of the PSPC field, used for RIXOS, could be imaged in four exposures. Additionally, short exposures of the central region of each PSPC field were made under photometric conditions, overlapping the corners of each of the four main images. This allowed us to derive accurate R magnitudes for candidates in all the fields.

The CCD imaging instrumentation available on the NOT was evolving rapidly during the RIXOS programme. Consequently a variety of cameras and formats were used, covering a region of sky between 1.5 and 3 arc minutes square with a pixel size of about 0.2 arcsec. The JKT CCD camera covered a field of view of about 6 arc minutes square, with a pixel size of approximately 0.3 arc seconds.

A limited number of deep exposures were obtained using a CCD camera mounted at the auxiliary focus of the WHT. This provided images of a 1 arc minute diameter region of sky which was recorded on a TEK 1024×1024 CCD chip at a spatial scale of 0.11 arcsec per pixel. Such exposures were interleaved with ISIS spectroscopy (which can be done with minimal overhead) to make deep images of selected fields during intervals of very good seeing.

3 CATALOGUE DESCRIPTION

The main RIXOS source catalogue is presented in Table 2. Column 1 contains the source name, formed from the position of the X-ray centroid. Column 2 provides the 90 per cent error in the X-ray position in arcseconds.

Columns 3 and 4 of Table 2 contain the position of the optical counterpart, except for clusters of galaxies and sources with no optical identification where the X-ray position is repeated. For point-like optical objects the positional accuracy is better than one arc second. The positions are derived from astrometry of the relevant POSS plate when the object is visible on it, or otherwise from a CCD image, using stars that are recorded on both the CCD image and the POSS to define a common frame. A plate solution of 6 parameters was adopted for small format CCD frames, and 12 parameters for the large format FORD CCD frames.

Columns 5 to 8 give the X-ray flux, the count rate, the total number of counts used to detect the X-ray source and the X-ray spectral slope of the source respectively. The first number in column 4 is the X-ray flux that was used to define the catalogue (from the counts given in column 7), based on a uniform spectral energy slope of –1 and with a (small) correction for Galactic absorption (see Table 1 for the Galactic absorbing column in the line of sight to each field centre). The second number in column 4 is the flux from our fit to the X-ray spectra of the sources (see Section 2 and Mittaz et al. 1999). For those sources with the lowest number of counts the best fit slope and flux have very large associated errors, but the corresponding values are also given for completeness. In a few cases (e.g. P700223-126, P700208-219 and P700216-265) the ROSAT observation was performed with spacecraft wobble switched off. This could lead in principle to incorrect estimates of the source fluxes if an average conversion factor between counts and flux is assumed. This is due to potential obscuration of the sources by the supporting wire grid, that would be different for each position in the detector. The fitted flux given in column 4 is obtained using the exposure map of each observation, that includes the effect of the supporting wire grid, so it is possible to estimate this effect by comparing both fluxes in column 4 for the point sources. The fluxes are very similar in most of the sources in these three fields with point-like counterparts, so this effect is probably not very important.

Column 6 contains the count rate (PHA channels 52-201) of the sources, estimated from 'cleaned' data from which observing segments with high background countrate and other bad data have been removed. These countrates are also corrected for vignetting (using the exposure maps).

The best fit power-law slope, along with the marginalised 1 sigma error, is given in column 8. It should be noted that the appropriateness of a power-law spectral approximation is a function of source type, and this is discussed more extensively in Mittaz et al. (1999).

A feature of the X-ray spectral fitting algorithm is that it assumes that the X-ray source is point-like, and it applies corrections for the energy-dependent point spread function of the ROSAT telescope accordingly. In contrast, the catalogue was defined on the basis of the integrated flux of extended sources. Thus for such sources, the spectral fit, count-rate and flux estimate refer to the centroid of the source only. This means that for extended sources (which by convention have a RIXOS source number, Sid, greater than 500) there is generally a significant discrepancy between the first and second numbers in the flux column (with the first column giving a more accurate estimate of the integrated source flux).

Column 9 gives the magnitude of the optical counterpart if there is one (or the integrated magnitude of the brightest cluster galaxy for cluster candidates). These are derived from a variety of sources depending on availability, and indicated by the symbol that precedes the magnitude. We have, however, attempted to maximise uniformity by quoting a number which refers to the R band or the closest approximation to it. Where we have calibrated R-band CCD images of the source we use those. Otherwise we use values derived from the POSS E plates, or (for sources not registered on the POSS E plates) a value estimated from our slit spectroscopy folded through the standard R-filter response. The accuracy of these 'slit magnitudes' is discussed by Puchnarewicz et al. (1996) and is found empirically to be within 30%. For bright stars (where the parameterised POSS data are inaccurate) or previously catalogued sources which were not re-observed by us, we quote catalogued magnitudes.

In column 10 we give, for AGN counterparts, the power-law slope that best represents the optical continuum spectrum (after removing lines and other features). The fitting procedure is discussed in more detail by Puchnarewicz et al. (1996) and its accuracy is generally limited by systematic effects to a value of about 50% in the slope. No attempt was made to fit a power-law to AGN whose optical spectrum exhibits a contaminating component due to the host galaxy.

Column 11 classifies the optical counterpart into one of five categories, Star, AGN, ELG, Clus or Gal (or blank for unidentified sources), while column 12 gives additional classification information where relevant. The classification 'ELG', for emission line galaxy, is used for any individual counterpart which has unresolved emission lines at redshift greater than zero, particularly if the lines are superimposed on a galaxy-like continuum. Broad-line objects are classified as 'AGN'. Isolated galaxies without emission lines are classified as 'Gal'. The number in parentheses following the cluster classification, 'Clus', is the number of galaxies measured at the cluster redshift. A colon indicates that the identification is uncertain. In the case of the 'Star' category all objects which have not been demonstrated to have chromospheric activity (based on the detection of CaII or Balmer emission lines in their spectrum) are formally marked as uncertain, though for bright stars the probability of chance association is very low, and the failure to detect chromospheric emission is probably due to its low equivalent width.

The redshift of extragalactic counterparts is listed in column 13. The emission lines upon which this is based are listed in column 14 for AGN and ELG counterparts. As an indicator of the spectral appearance, Column 15 gives the FWHM of one of the lines, underlined in column 14, in units of 1000 km/s and rounded down to the nearest 1000 km s^{-1}. For maximum uniformity, preference is given to Hβ or MgII when these are available and well defined.

Column 16 indicates whether ancillary information is available on the source. An 'N' indicates that there is a note on the source in section 3.2. A 'C' marks sources which have catalogue cross-references in Table 3, whereas an 'I' means that there is a CCD image of the field (see section 3.1).

The final column of the Table (number 17) contains a cross-reference to the field number and source number as defined internally within the RIXOS programme and used in other publications to refer to RIXOS sources (Puchnarewicz et al. 1996, Puchnarewicz et al. 1997, and Mittaz et al. 1999). The field number (Fid) is the same as that in column 1 of Table 1.

The contents of this Table are available on http://www.mssl.ucl.ac.uk/www_astro/rixos.html. Data on the RIXOS AGN are available in the NASA Extragalactic Database.

3.1 Images and Finding Charts

An optical 'finding chart' for each RIXOS source is contained in Fig. 3, based on the parameterised POSS-E data. Each chart shows a region of sky two arc minutes square that is centered on the X-ray centroid. The 90% confidence error circle is defined by the gap in the 'crosshairs', and the position of any optical counterpart or counterparts is indicated by tick marks. Inthe case of extended sources where the errors aare not statistical, no crosshairs are shown.

Fig. 4 shows selected CCD images of RIXOS sources, specifically those where the CCD image adds to the information available from the POSS charts alone (the most obvious example being cases where the optical counterpart is not visible on the POSS). The region of sky depicted is 1 arc minute square in the case of the CCD images. This is generally centered close to the X-ray centroid, but in some cases the region shown is offset significantly from the centre in order to show specific features, or to establish the location of the CCD image with respect to the POSS chart by including objects in common.

3.2 Notes on individual sources

RX J001002.5+110837: This catalogued bright star produces a blank finding chart, so we have chosen not to plot it.

RX J014250.2+041358: A single, very broad feature at 6220Å is identified as MgII. There is possible CIII] emission at 4200Å but the spectrum is noisy at this wavelength.

RX J014300.9+042202: Pointlike X-ray source. The tentative ID is a z=0.135 galaxy which lies about 7 arcsec north of the X-ray position (Fig. 4). The pointlike optical object which is a similar distance to the south of the X-ray position is a late-type star, as is the object of similar brightness which lies to the north-east. There is a faint optical object very close to the X-ray position, but its colours appear unremarkable on U, B and R CCD images.

RX J020701.9+151502: The object close to the X-ray position (Fig. 4) which lies to the south-east of the relatively bright star seen on the POSS (which is of late type) is UV bright on CCD images relative to other objects in the field and is a likely ID.

RX J020706.8+150455: A UV-bright object close to the X-ray position, the brightest object visible in the image of the field contained in Fig. 4, is the probable ID, but no spectrum is available.

RX J040546.8–131110: A pointlike X-ray source. The single optical spectrum of the object centered in the error circle shows a blue continuum, with a possible emission line at 5400Å which coincides with the join between the blue- and red-arm ISIS spectra. Classified as a possible AGN at unknown redshift.

RX J040621.3–130340: The object closest to the X-ray position appears slightly extended on an R-band CCD image.

RX J041612.1+011432: The tentative stellar ID is about 20 arcsec from the X-ray position.

RX J072047.8+710945: Initially considered a single extended X-ray source, this is actually two. There is a star with a flux of 4.7×10^{-14} erg cm^{-2} s^{-1} to the north-west of the X-ray position, and a z=0.23 cluster of galaxies with a flux of 2.1×10^{-13} erg cm^{-2} s^{-1} (0.5-2.0 keV) which is centered to the south-east of the catalogued X-ray source. This cluster is in turn about one Abell radius north of the cluster A 574

RX J085340.3+134927: A likely ID is the Seyfert 2 galaxy which lies towards the edge of a relatively large X-ray error circle. However there is also an Hα emission line galaxy at the same redshift in the error circle (RA(2000) 08h 53m 41.02s Dec(2000) +13° 49′ 19.2″), together with several other fainter objects which have not been observed spectroscopically. It is thus also possible that we are seeing compact cluster emission, though there is no evidence that the X-ray emission is extended. This is also an EMSS source, where the ID is listed as the Sy 2.

RX J085345.5+134948: The bright A-type star is itself an unlikely ID. The correct ID is probably a faint companion, or an unrelated line of sight object.

RX J085825.9+135724: An overdensity of galaxies on the CCD image in the vicinity of the X-ray source (Fig. 4) suggests probable cluster emission but no spectroscopy is available.

RX J090517.8+335004: Complex X-ray source, with the two main components separated by ∼40 arcsec and aligned approximately north-south. There are four (or five?) counterparts within the X-ray error circle. The northernmost is a star, while the nature of the others is unknown. This is a potential compact galaxy group.

RX J091049.4+430407: There is a radio source less than an arc minute from the X-ray position. However the X-ray image is complex and is probably of two X-ray sources separated by ∼ 30 arcsec, aligned with a position angle of approximately 140 deg. A deep WHT R-band image of the X-ray position is blank.

RX J094427.0+164630: Extended diffuse X-ray source, possible cluster candidate, but no spectroscopy done.

RX J100120.3+555349: Gravitationally lensed quasar [HB89] 0957+561 (Hewitt & Burbidge 1989). Considered as a single X-ray source.

RX J100454.8+050418: Diffuse X-ray emission, probably associated with the galaxy that is listed as the optical counterpart.

RX J100851.6+524553: Suggested ID is the brighter (most westerly) of a close stellar pair.

RX J101010.4+515817: Apparently diffuse X-ray source which is either a collection of faint point sources (all individually below our survey limit) or a low surface brightness extended object. There is no obvious optical counterpart.

RX J101052.2+533821: This is a K4 star. It has a fainter M companion 11 arcsec to the north and 11 arcsec to the west.

RX J101125.6+543921: This is a complex X-ray source with at least two components. There are a number of possible optical counterparts, these being a pair of stars approximately 40 arcsec to the north-west of the X-ray centroid (not resolved on the parameterised POSS chart), a galaxy at z=0.044 approximately 1 arcmin to the south-east of the X-ray centroid, and a fainter Hα emission line galaxy which is close to the centre of the X-ray error circle. All may contribute flux, though the centroid of the X-ray emission favours the two galaxies.

RX J101136.1+514714: Diffuse X-ray source.

RX J102442.3+465227: Close stellar pair. The shape of the X-ray contours suggests that this is actually two X-ray sources, one corresponding to each star.

RX J111730.1+074618: The most probable ID is a cluster of galaxies at redshift 0.16, however there is also a 17^{th} magnitude z=0.136 HII region galaxy about 30 arcsec north of the X-ray centre (PA ∼ 350°).

RX J111809.9+212554: Probably at least two X-ray sources with a separation of approximately 1 arcmin at a PA of 135°. The catalogued X-ray position is the centroid of the emission. The object to the north-west of the X-ray centroid is an M star.

RX J112018.4+135216: Close pair of stars.

RX J112524.9+542221: This is a pair of optically active M stars, thus we have considered this to be two X-ray sources.

RX J120049.1–032738: We believe this to be a cluster based on the X-ray image, which is very diffuse. The estimated diameter is 2 arcmin. We have probable redshifts for 3 galaxies, two at z=0.39 and the other at z=0.28. Thus, if this is a cluster, the redshift is ambiguous.

RX J120110.8–033702: The X-ray source is extended with a flattened morphology. The pair of objects about 30 arcsec to the north-east of the X-ray centroid are both stars. The object to the west is double, one component of which is a galaxy at redshift 0.211. There are other plausible galaxies in the optical image of similar magnitude, thus this remains a cluster candidate.

RX J120330.7+275532: The galaxy to the west of the suggested ID exhibits narrow Hα/[NII] emission at a redshift of 0.142.

RX J121828.6+301150: Diffuse X-ray emission which may be a cluster at z∼0.36 (based on one galaxy, closest to the X-ray centroid) with a probable point source embedded. The point source may be an M star 20 arcsec to the south-west of the X-ray centroid but the estimated X-ray flux of the star in isolation would place it below the RIXOS3 threshold.

RX J122135.6+280613: Lyman forest absorption plus Lyman edge detected.

RX J123138.1+202526: The object closest to the X-ray position on the POSS E chart is not detected in our CCD images and is probably not real. Thus, the M5 star is the closest object to the X-ray position and is a probable ID.

RX J123154.9+195309: The X-ray source is elongated with PA ∼ 45° with the emission concentrated to the north-east. Two optical objects have been observed: the one 30 arcsec to the west of the X-ray centroid is a star, while the object 20 arcsec to the north-east is an AGN at z=0.142 with broad Hα emission. There is probably significant X-ray emission from the AGN, but the extended emission could be from a cluster of galaxies at unknown redshift. The X-ray source is formally coincident with the radio source 4C +20.30. However the 4C source has a large positional uncertainty. The NVSS shows a source (NVSS J123153.2+194947) with a consistent radio spectral index which is likely to be the origin of the emission recorded in the 4C catalogue. The NVSS source is however several arc minutes from the RIXOS X-ray source and thus it is unlikely that the radio and X-ray sources are related.

RX J125738.4+472759: Visual binary system. However, the X-ray contours favour the G8 star as the X-ray candidate, so we have considered this as a single X-ray source.

RX J131058.8+323335: A variable optical and radio source discussed by Machalski & Engels (1994).

RX J133146.3+105653: The star has a visual companion, about 2 magnitudes fainter than it and located to the south-east.

RX J141231.5+435539: The majority of the X-ray emis-

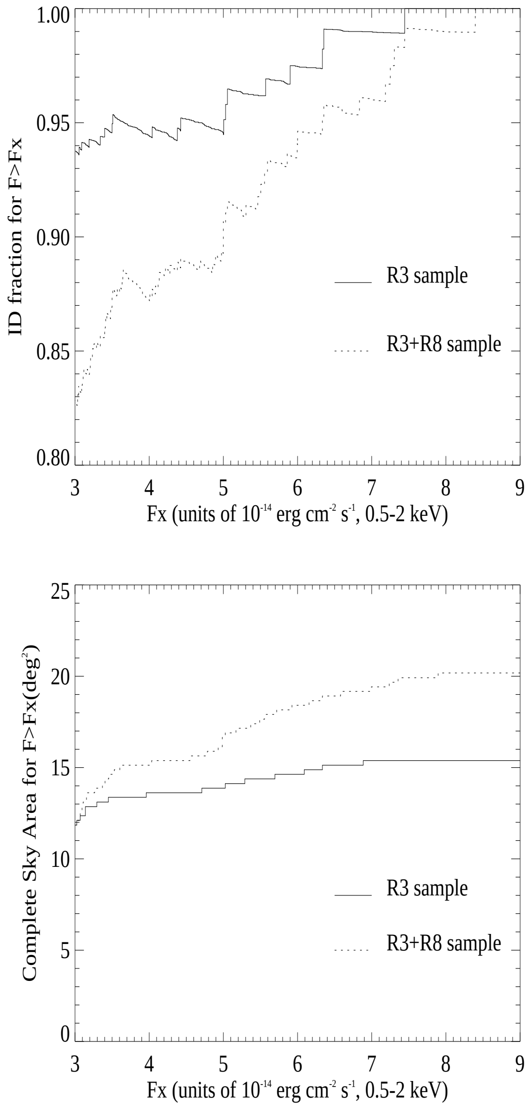

Figure 5. *Above:* The identified fraction of RIXOS sources above a give flux threshold. Data are plotted for the RIXOS3 sample alone, and for the combined RIXOS3 and RIXOS8 sample. *Below:* The sky area over which identifications are complete as a function of flux threshold. Again separate curves are plotted for the RIXOS3 sample alone, and for the combined RIXOS3 and RIXOS8 sample.

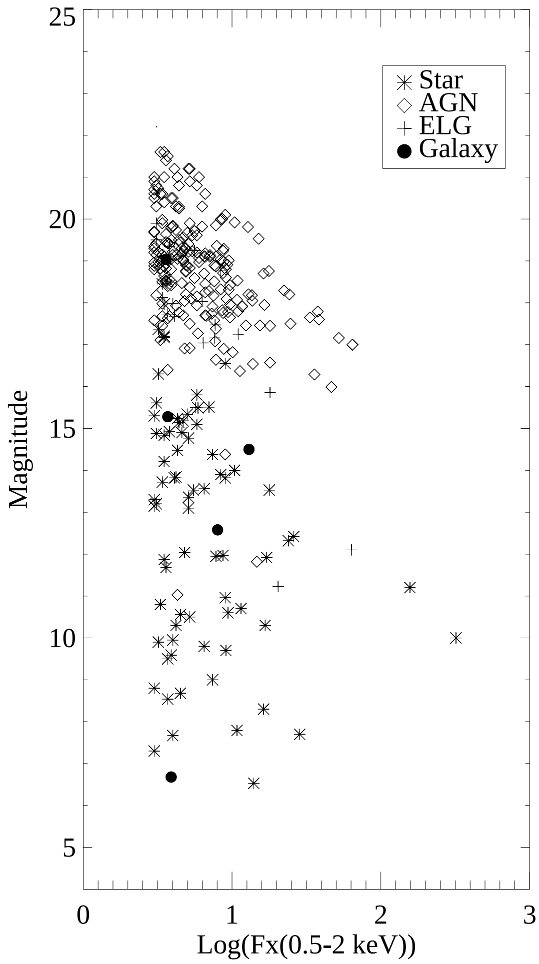

Figure 6. Optical (R) magnitude versus the logarithm of the 0.5-2.0 keV X-ray flux for various classes of identified RIXOS sources. The X-ray flux is expressed in units of 10^{-14} erg cm^{-2} s^{-1}.

sion is centred on the indicated Sy2 galaxy (also catalogued as IRAS14105+4409). However there is also a close pair of Hα emission line galaxies (z=0.13) about 30 arcsec to the north-west of the X-ray centroid, and visible at the edge of the CCD image in Fig. 4.

RX J142754.6+330003: The AGN is seen through the disk of a z$\sim$0.1 foreground galaxy whose nucleus lies about 7 arcsec to the east of the AGN.

RX J161418.8+654854: A pointlike X-ray source. There are no obvious optical counterparts in the X-ray error circle, even in the deep WHT image. A possible genuine blank field.

RX J162902.3+372434: Double quasar. Again, we have considered this to be a single physical X-ray source.

RX J163616.7+570644: A ROSAT HRI image reveals a pointlike X-ray source at a position consistent with that of the POSS object close to the PSPC position. The PSPC and HRI fluxes are consistent with one another.

RX J172904.4+742552: A close pair of optically active M stars. We have counted this as two different physical X-ray sources.

RX J180603.7+694024: This is close to an EMSS source which is identified as a z=0.461 AGN in Stocke et al. (1991). However this AGN is inconsistent with the RIXOS position (it is the object at PA$\sim$15° just within the northern edge of our POSS finding chart) and is also outside the EMSS error circle. The suggested RIXOS ID (a z=0.321 Seyfert galaxy) is close to the centre of the RIXOS error circle and is also consistent with the EMSS position. A spectrum of the RIXOS ID taken on the Keck telescope by Hasinger (unpublished) reveals broad Hα.

RX J180823.7+694208: A pointlike X-ray source. The suggested counterpart is a blue object which may have narrow Hα and [OIII] emission lines, though the spectrum is of poor quality. The redshift is 0.17 if these line identifications are correct. The object $\sim$20 arcsec to the west of this is a

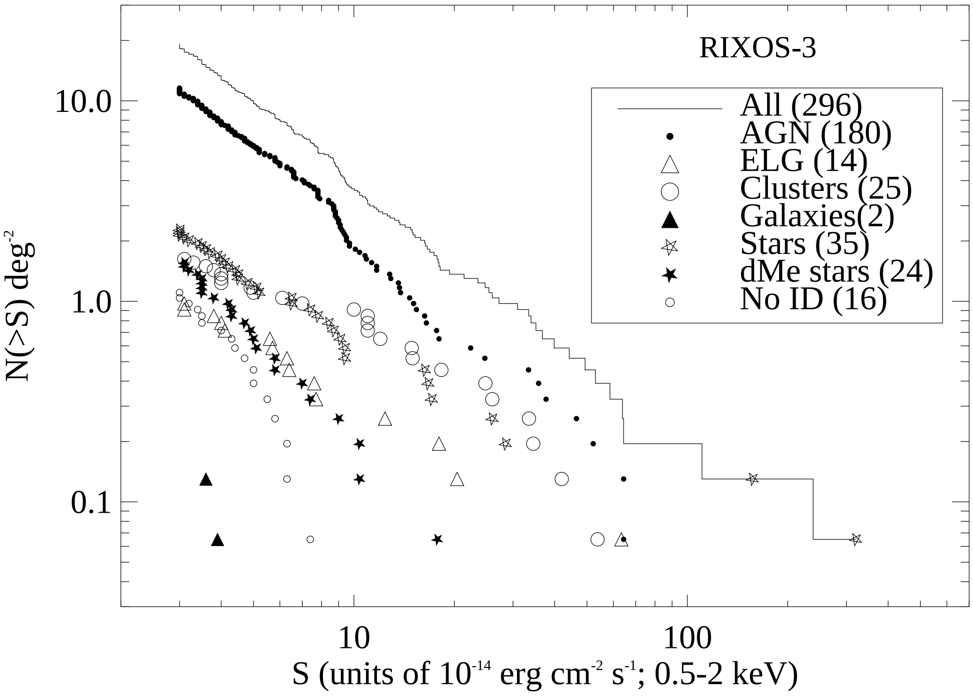

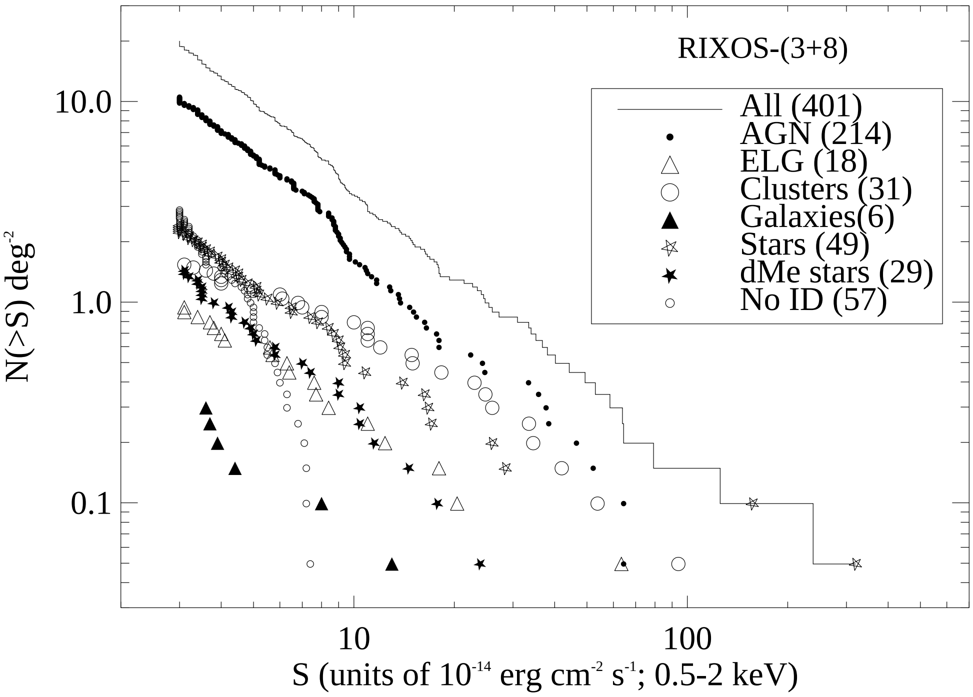

Figure 7. Log N - Log S distributions for various classes of sources in the RIXOS survey. The upper plot shows results from the RIXOS3 sample alone, while the lower plot shows data from the total sample which includes both RIXOS3 and RIXOS8 fields. The number of objects in each category is listed within parentheses in the legend.

late-type star which shows no evidence of activity. The object ~20 arcsec to the south-east of the candidate is a galaxy at a redshift of 0.41.

RX J231303.7+104914: The error circle of this X-ray source contains two AGN at different redshifts (1.333 and 0.715). This has been treated as two different X-ray sources.

4 SURVEY STATISTICS

As noted previously, 82 ROSAT fields were used in the optical work on the RIXOS survey. In 64 of these fields, all X-ray sources brighter than the survey flux limit of 3×10^{-14} erg cm^{-2} s^{-1} were examined during the spectroscopy programme (though not all were successfully identified). Work on the remaining 18 fields is complete to a higher flux level of $\sim 8 \times 10^{-14}$ erg cm^{-2} s^{-1} but only partially complete below this. We refer to the 64 fields that have been searched down to 3×10^{-14} erg cm^{-2} s^{-1} as the RIXOS3 sub-sample, and the remaining 18 fields as the RIXOS8 sub-sample. The area surveyed in each ROSAT pointing is about 0.25 deg^2. Thus RIXOS3 covers a sky area of 15.77 deg^2, with the RIXOS8 sub-sample adding a further 4.44 deg^2, to a total area of 20.21 deg^2.

The RIXOS survey as a whole contains 401 X-ray sources brighter than 3×10^{-14} erg cm^{-2} s^{-1}, of which 296 are in RIXOS3 fields, and 105 are in RIXOS8 fields. Figure 3 provides finding charts for the 396 X-ray sources originally detected in these fields (except for RX J001002.5+110837, see Section 3.2). In the course of the survey, five of these sources were found to be actually two X-ray sources very close together (RX J072047.8+710945, RX J102442.3 +465227, RX J112524.9+542221, RX J172904.4+742552, RX J231303.7+104914, see Section 3.2), taking the total number of different X-ray sources to 401, as quoted above. We have included in Table 2 one line for each one of these two counterparts. Furthermore, two of the X-ray sources found in this survey coresponded to double quasars (RX J100120.3+555349 and RX J162902.3+372434). We have given in Table 2 the optical data for both members of each pair, but we have chosen to consider each one of these pairs a single physical X-ray source. Finally, we have also included a line for each one of the two stars that are near the position of RX J125738.4+472759, although we believe that only one of them is the real counterpart (see Section 3.2). In total, the 396 originally detected X-ray positions, plus the 8 X-ray sources with two entries make the total of 404 lines in Table 2.

In the upper panel of Fig. 5 we plot the fraction of sources brighter than a given flux that have been identified for the RIXOS3 fields alone, and for the full survey (RIXOS3 + RIXOS8). It is seen that 94% of sources with fluxes greater than 3×10^{-14} erg cm^{-2} s^{-1} have been identified in RIXOS3. In the combined sample the corresponding number is 83%.

We can also describe the completeness of the survey based on the brightest source in each field that remains unidentified. This can occur either because we failed to confirm a counterpart (generally the case in RIXOS3) or because the source was not worked on in the spectroscopic programme (as is the case for a number of sources in RIXOS8). We can thus plot the effective area of sky that is completely identified above a given X-ray flux as a function of flux, shown in the lower panel of Fig. 5.

The optical (R) magnitude of point-like optical counterparts is plotted against their 0.5-2.0 kev X-ray flux in Fig. 6. The faintest AGN counterparts have R$\sim$22 at the survey flux limit. The well defined upper boundary of optical magnitude versus X-ray flux for AGN presumably reflects the limited range of X-ray to optical flux ratio in this class of object.

5 NUMBER COUNTS

The integrated log N - log S curves ($N(>S)$) are shown in Fig. 7, for both the RIXOS3 sample (upper panel) and all RIXOS sources above a flux of 3×10^{-14} erg cm^{-2} s^{-1} (lower panel). A single power-law fits well the total differential log N - log S curves, yielding a slope of 2.6 ± 0.3. Previous studies of the 0.5–2 keV $N(>S)$ curve with ROSAT used a broken power-law model for fitting, finding a break below our flux limit ($\sim 2-3 \times 10^{-14}$ erg cm^{-2} s^{-1}). Our single power-law slope is hence directly comparable to the power-law slope above the break in those studies. Our sample partially overlaps with that of Hasinger et al. (1993), so it is hardly surprising that the slope above the break of their broken power-law fit is compatible with ours (2.72 ± 0.27). Branduardi–Raymont et al. (1994) used a different sample (but again containing some fields also used in RIXOS), obtained from the United Kingdom Deep and Medium Surveys (McHardy et al. 1998, Carballo et al. 1995). The slope of the 'bright branch' of their $N(>S)$ fit is very similar to ours ($2.64^{+1.19}_{-0.52}$), although with larger uncertainties due to their lower number of sources.

The $N(>S)$ curves for the different types of sources in both samples are also included in Fig. 7. It is clear from that figure that AGN dominate the source counts below a flux of $\sim 10^{-13}$ erg cm^{-2} s^{-1}, making up about 50 per cent of the total number of sources. Comparing the $N(>S)$ of our clusters with that of Rosati et al. (1995), we find approximately a factor of 2 less clusters at our flux limit than they do (we find ~ 1.2 deg^{-2} while they find ~ 2.4 deg^{-2}). This is probably because our detection algorithm was optimized for the detection of point sources (or at least unresolved sources down to the angular resolution of ROSAT), and the visual inspection of 'clusters' of point sources only picked up very bright nearby extended clusters, so we very likely missed an important fraction of distant fainter clusters. Nevertheless, the slope of our best fit to the RIXOS3 cluster sample (2.1 ± 0.9) is similar to theirs (~ 2) albeit with a large uncertainty.

Stars and clusters have similar densities at our flux limit. The less abundant types of sources are 'normal' galaxies and ELGs. The total number of both types of sources are at the level or below the number of unidentified sources, making definitive statements about their global properties difficult from RIXOS-sized samples, as emphasized by Page et al. (1997a). As expected, the fraction of unidentified sources increases strongly at the faintest flux levels, where the faintness of the optical counterparts and the presumably worse position determinations from X-rays conspire to make a definitive identification more difficult.

6 SUMMARY AND CONCLUSIONS

This paper presents the RIXOS catalogue, a medium sensitivity flux-limited survey of X-ray sources detected in ROSAT PSPC fields together with optical identifications to a high level of completeness. The scientific content of the survey has been explored in a number of papers which make use of RIXOS catalogue data. In an early study Castander et al. (1995) discussed the implications for the evolution of X-ray selected galaxy clusters (though the relatively crude manual selection of extended sources used in RIXOS has since been superseded by superior techniques; Burke et al. 1997, Scharf et al. 1997). The evolution of the X-ray luminosity function of AGN has been considered in detail using a combination of RIXOS and Einstein Extended Medium Survey data in Page et al. (1996), work that was extended to include data from a ROSAT deep survey in Page et al. (1997b). The evolution of narrow emission-line galaxies has also been discussed, in Page et al. (1997a). The X-ray and optical continuum properties of RIXOS AGN have been analysed in Puchnarewicz et al. (1996), while AGN with a very red optical continuum are discussed further in Puchnarewicz & Mason (1998). This work is extended to include the optical and UV emission line properties in Puchnarewicz et al. (1997). The X-ray spectral properties of RIXOS sources, including sources in RIXOS fields fainter than the formal survey flux limit, are considered in Mittaz et al. (1999). The clustering of RIXOS AGN has been studied by Carrera et al. (1998). One Individual RIXOS source of interest is discussed in Puchnarewicz, Mason & Carrera (1996).

There may be minor differences between the data used in the above publications and those reported in the present catalogue, due to additional information or improved quality control. In general the information presented in the present work supersedes that in earlier papers.

ACKNOWLEDGMENTS

The RIXOS project has been made possible by the award of International Time on the La Palma telescopes by the Comité Científico Internacional. This research has made use of data obtained from the Leicester Data Archive Service (LEDAS) and we especially thank Steve Sembay for his kind assistance. We thank the Royal Society for a grant to purchase equipment essential to the RIXOS project. FJC, XB, RC and JIGS thank the DGES for financial support, under project PB95-0122. The INT, JKT and WHT are operated on the island of La Palma by the Isaac Newton Group in the Spanish Observatorio del Roque de los Muchachos of the Instituto de Astrofísica de Canarias. The NOT is operated by the Nordic Optical Telescope Scientific Association in the Spanish Observatorio del Roque de los Muchachos. This research has made use of the NASA/IPAC Extragalactic Database (NED) which is operated by the Jet Propulsion Laboratory, California Institute of Technology, under contract with the National Aeronautics and Space Administration. It also made use of the Lyon-Meudon Extragalactic Database (LEDA) maintained at CRAL, Lyon, France.

REFERENCES

Boyle B.J., McMahon R.G., Wilkes B.J., Elvis M. 1995, MNRAS, 272, 462.
Branduardi-Raymont G., et al., 1994, MNRAS, 270, 947
Burke D.J., Collins C.A., Sharples R.M., Romer A.K., Holden B.P., Nichol R.C., 1997, ApJL, 488, 83.
Carballo R., Warwick R.S., Barcons X., González Serrano J.I., Barber C.R., Martínez-González E., Pérez-Fournon, J.Burgos, 1995, MNRAS, 277, 1312
Carrera F.J., Barcons X., Fabian A.C., Hasinger G., Mason K.O., McMahon R.G., Mittaz J.P.D. , Page M.J., 1998, MNRAS, 299, 229
Cash W., 1979, ApJ, 228, 939.
Castander F.J., et al. 1995 Nature 377, 39.
David F.R., et al., 1996, in: The ROSAT Users Handbook, U. Briel et al., eds.
Hasinger G., Burg R., Giacconi R., Hartner G., Schmidt M., Trümper J., Zamorani G., 1993, A&A, 275, 1.
Hasinger G., Johnston H., Verbunt P., 1994a, A&A, 288, 466.
Hasinger G., et al., 1994b, Legacy, 4, 40, MPE/OGIP Calibration Memo CAL/ROS/93-015.
Hasinger G., Burg R., Giacconi R., Schmidt M., Trümper J., Zamorani G., 1998, A&A, 329, 482.
Hewitt A., Burbidge G., 1989, ApJS, 69, 1
Lewis G., & Irwin M. 1996, Spectrum, Newsletter of the Royal Observatories, 12, p22.
Machalski J., Engels D., 1994, MNRAS, 266, 69P.
McHardy I.M., et al. 1998, MNRAS, 295, 641.
Mittaz J.P.D., et al. 1999, MNRAS, 308 233
Page M.J. et al. 1996 MNRAS 281, 579.
Page M.J., Mason K.O., McHardy I.M., Jones L.R., & Carrera F.J. 1997a MNRAS 289, 693.
Page M.J., Mason K.O., McHardy I.M., Jones L.R., & Carrera F.J. 1997b MNRAS 291, 324.
Puchnarewicz E.M., et al. 1996 MNRAS 281, 1243.
Puchnarewicz E.M., Mason K.O., & Carrera F.J., 1996 MNRAS 283, 1311.
Puchnarewicz E.M., et al. 1997 MNRAS 291, 177.
Puchnarewicz E.M., & Mason K.O. 1998 MNRAS 293, 243.
Rosati P., Della Ceca R., Norman C., Giacconi R., 1998, ApJ, 492, L21
Scharf C.A., Jones L.R., Ebeling H., Perlman E., Malkan M., Wegner G., 1997, ApJ, 477, 79.
Shanks T., Georgantopoulos I., Stewart G.C., Pounds K.A., Boyle B.J., Griffiths R.E. 1991, Nat., 353, 315.
Stark A.A., Gammie C.F., Wilson R.W., Bally J., Linke R.A., Heiles C., Hurwitz M., 1992, ApJS, 79, 77
Stocke J.T., et al., 1991, ApJS, 76, 813.
Trümper J. 1983 Adv. Space Res. 4, 242.
Voges W. et al. 1998, A&A, 349, 389
Zimmermann H.U., et al., 1994, MPE Report, 257.

This paper has been produced using the Royal Astronomical Society/Blackwell Science TEX macros.

Figure 3. Optical finding charts for each RIXOS source derived from parameterised POSS-E data measured with the APM at Cambridge. Each chart shows a region of sky two arc minutes on a side centered on the X-ray position. The 90% confidence error circle is defined by the gaps in the 'crosshairs'. In the case of extended sources where the errors are not statistical, no crosshairs are shown. The position of optical counterparts is indicated by tick marks. For visual simplicity, no distinction is made between stellar and extended objects.

Figure 4. CCD images of selected RIXOS sources (see Table 2). A region of sky 1 arc minute on a side is shown in each image. This is generally centered close to the X-ray centroid, but in some cases the region shown is offset significantly from the centre in order to show specific features, or to establish the location of the CCD image with respect to the POSS chart by including objects in common. Optical counterparts are indicated by tick marks.